

# NUMERICAL ANALYSIS OF FRACTURE OF PRE-STRESSED FERROELECTRIC ACTUATOR TAKING INTO ACCOUNT COHESIVE ZONE FOR DAMAGE ACCUMULATION

**S.Kozinov, M.Kuna**

Institute for Mechanics and Fluid Dynamics, TU Bergakademie Freiberg  
Lampadiusstraße 4, 09596, Germany  
Sergii.Kozinov@imfd.tu-freiberg.de, Meinhard.Kuna@imfd.tu-freiberg.de

**Keywords:** Finite element method, Ferroelectric actuator, Fracture mechanics, Domain switching, Cohesive zone model.

**Summary:** *Operational safety of smart-structures as well as ferroelectric multilayer actuators (MLA) is essentially reduced by crack formation. Such failure processes are numerically simulated in this work by the finite element method (FEM) employing coupled electro-mechanical 3D analyses. At first, the poling process during manufacturing the actuator is simulated. During this step, the pre-stress due to the presence of an external frame which protects the MLA against tensile forces is obtained. After the end of the poling process, an alternating electric loading with constant amplitude is applied. In order to model the bulk material behavior, ferroelectric user elements are implemented into the commercial software ABAQUS, thus allowing to simulate poling process of the actuator as a result of the micromechanical domain switching. Material damage is accumulated in accordance with the traction-separation law (TSL) of an electro-mechanical cyclic cohesive zone model (EMCCZM). The cohesive zone technique allows to capture initiation and accumulation of damage, while domain switching modeling ensures a realistic simulation of the non-linear processes occurring in the ferroelectric material. In the cohesive zone, a finite electric permittivity is assumed, which degrades with damage accumulation. Another important feature is that applied cyclic loading of a constant amplitude leads to increasing damage which can not be modeled with a monotonous TSL. The results of the numerical simulation qualitatively coincide with the experimentally observed patterns of crack initiation. It was found that the poling process of ceramics may induce cracking at an electrode surface which further develops under purely electric cyclic loading. Damage evolution is observed due to mechanical and electrical field concentrations near the electrode tip. To the authors' knowledge, it is the first analysis dealing with coupled ferroelectromechanical modeling combined with damage accumulation in smart structures. Such simulations are an important step towards future optimizations of the actuator design.*

## 1. INTRODUCTION

Piezo-(ferro-)electric multilayer actuators (MLA) are widely used in the field of high-precision positioners due to their accuracy, high stiffness, large generative forces and fast response [1]. A

present-day multilayer actuator consists of hundreds of ceramic layers aggregated with internal electrodes, which terminate inside the ceramics. High electrical fields or local stress concentrations in the vicinity of the electrode edge, originating during actuators exploitation, make it necessary to correctly predict fracture of such smart devices. Profound reviews about cracking in ferroelectric ceramics can be found in [2, 3].

Piezoelectric actuators show the non-linear electromechanical behavior of ferroelectric bulk ceramics due to the domain-switching phenomenon caused by the high electric field concentration. Early finite element method (FEM) simulations of actuators mostly focused on the modeling of linear piezoelectric systems, which is a rough approximation of inherent nonlinear electromechanical properties of ferroelectrics. Moreover, in most of them, the domain distribution and electromechanical fields are not fully coupled and only the former depends on the latter. In the present investigation a micromechanical material model, based on tetragonal volumetric domain switching in a single crystal [4], is used.

The crack propagation mechanisms in the actuators are still not clear due to the complex non-linear interactions between electromechanical fields and microstructure near the electrode edge. Lack of accurate experimental data is due to several reasons. The strains found from strain gages are only average values in the local area due to the large size of gages in comparison with the thickness of ceramic layers. Therefore deformations near the electrode edge can not be precisely measured. On the contrary, interferometry only provides limited pattern information in the small region near the electrode edge.

In general, experimental observations indicate that the electric-field induced cracks initiate substantially from the electrode edge and they can propagate along the ceramic–electrode interface [5, 6, 7]. The concept of cohesive zone models is quite efficient to simulate initiation and evolution of damage and cracking, when one or several possible damage paths with embedded cohesive elements can be introduced a priori, as, for example, along interfaces in polycrystalline ceramics. A first adaptation of the classical exponential cohesive zone model to ferroelectric materials for electric fatigue simulation was done by Arias et al. [8], though some physical simplifications were made. Other simulations with cohesive zone elements but with piezoelectric bulk behavior were performed by Utzinger et al. [9] and Verhoosel and Gutiérrez [10].

The coupled electromechanical cyclic cohesive zone model (EMCCZM) was suggested by Kozinov et al. [11] as an extension of the previously developed by Roth et al. [12] pure mechanical cyclic cohesive zone elements. Both mechanical and dielectric properties of the material during its ongoing degradation are taken into account in EMCCZM. It allows to track initiation and evolution of the interface cracks during mechanical and/or electrical loading, applied to simple structures and actuators. Damage accumulation is captured resulting from the electromechanical response of the actuators during operational loading.

Pioneering study of multilayer actuator response incorporating the simulation of a ferroelectric behavior was done by Kamlah and Boehle [13]. Subsequent papers by Zhao et al [7] and Abdollahi and Arias [14] offered improvements and modifications, as well as simplifications.

The first fully coupled electromechanical simulation of the MLA, considering ferroelectric bulk material behavior together with the cohesive zone implementation, was recently presented

by the authors [15].

The outer frame, leading to the pre-stressing of the MLA, ensures a longer lifetime and better performance of the actuators. The pre-stressed MLA's performance study is needed in order to optimize their operation. To the authors' knowledge such a fully coupled electromechanical simulation of the bulk material behavior with a cohesive zone implementation for damage accumulation is done for the first time. It enables the study of electromechanical fields in the critical regions of a MLA and investigation of a possible gradual failure.

## 2. Ferroelectric materials constitutive behavior and electromechanical cyclic cohesive zone model

For a detailed explanation about EMCCZM as well as the constitutive behavior of ferroelectric materials the reader is referred to [11]. In this section only a brief overview is provided.

Constitutive behavior of a piezoelectric material with remanent strain  $\epsilon_{kl}^r$  and remanent polarization  $P_i^r$  in a fixed rectangular coordinate system  $x_k (k = 1, 2, 3)$  is formulated by the following equations:

$$\sigma_{ij} = C_{ijls}(\epsilon_{ls} - \epsilon_{ls}^r) - e_{sij}E_s, \quad D_i = e_{ils}(\epsilon_{ls} - \epsilon_{ls}^r) + \kappa_{is}E_s + P_i^r. \quad (1)$$

where  $u_k, \epsilon_{ls}, \phi, \sigma_{ij}, D_i, E_i$  are mechanical displacements, strains, electric potential, mechanical stresses, electric displacements and electric field, respectively.

Domains are subregions of a grain, in which all dipole moments of the neighboring unit cells are aligned and have identical spontaneous strain  $\epsilon_{kl}^{sp}$  and spontaneous polarization  $P_i^{sp}$  (Fig.1, left). During application of a strong electric loading (Fig.1, center) domains orient along the direction of the electric field. After termination of the external electric loading a remanent polarization  $P^r$  as well as a remanent strain  $\epsilon^r$  remain (Fig. 1, right).

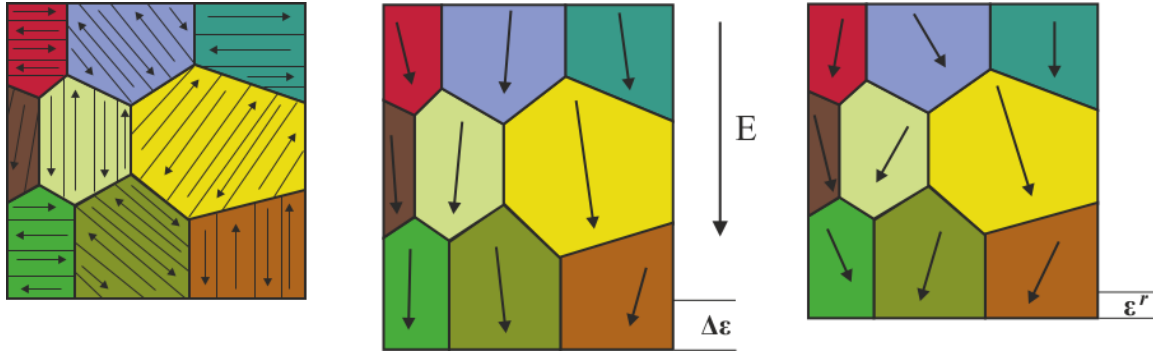


Figure 1. Reorientation of the domains during poling process ( $\Delta\epsilon$  – strain in a representative polycrystalline volume element,  $\epsilon^r$  - remanent strain, homogenized over the polycrystal).

According to the nonlinear evolution law defined by Eqs. (1), the strain hysteresis (Fig. 2) as well as the polarization hysteresis (Fig. 3) can be reproduced in consequence of domain switching.

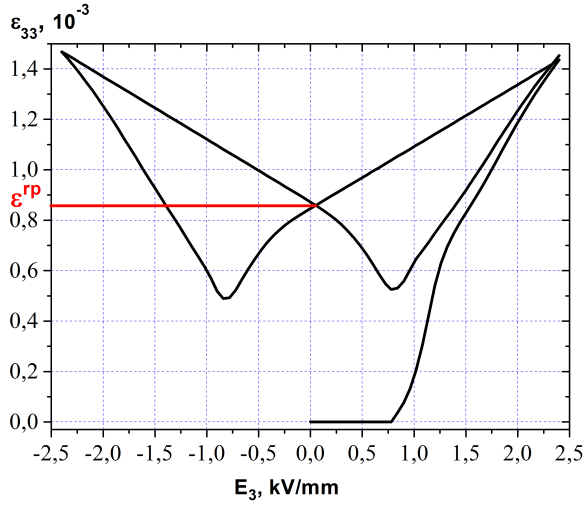


Figure 2. Strain hysteresis loop.

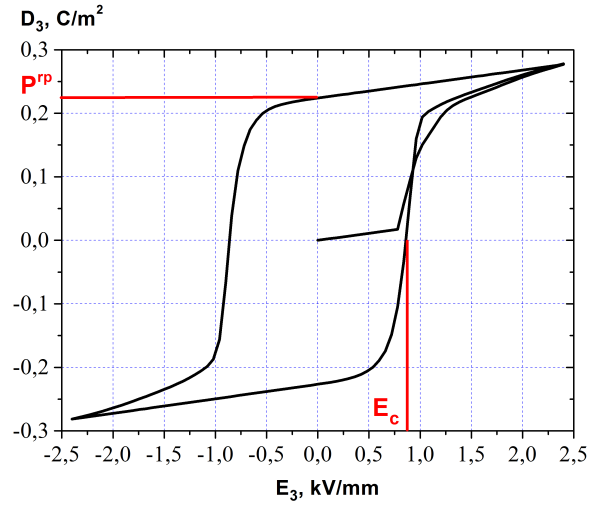


Figure 3. Polarization hysteresis loop.

Ferroelectric domain switching happens when the critical work barrier [2]

$$\omega_c^{\pm 90^\circ} = \sqrt{2}P^{sp}E_c, \quad \omega_c^{180^\circ} = 2P^{sp}E_c \quad (2)$$

is overcome by the energy supply [16]

$$\sigma_{ij}\epsilon_{ij} + \sigma_{ij}\Delta\epsilon_{ij}^{sp} + E_i D_i + E_i \Delta P_i^{sp} \geq \omega_c^\alpha, \quad \alpha \in \{-90^\circ, 90^\circ, 180^\circ\}. \quad (3)$$

For tetragonal domains two types of switching are possible: 90° switching, altering both spontaneous strain and polarization, and 180° switching, leading to spontaneous polarization change with no influence on the spontaneous strain value. This micromechanical ferroelectric model was implemented as user routine for the finite element code Abaqus<sup>®</sup>.

For a lead zirconate titanate PZT-5H the linear material properties used for the numerical modelling are presented in Table 1, while the nonlinear ferroelectric quantities are shown in Table 2.

elastic moduli (MPa)					
$C_{1111}$	$C_{2222}, C_{3333}$	$C_{1122}, C_{1133}$	$C_{2233}$	$C_{1212}, C_{1313}$	$C_{2323}$
117000	126000	53000	55000	35300	35500
dielectric constants ( $\mu\text{F}/\text{m}$ )			piezoelectric constants ( $\text{C}/\text{m}^2$ )		
$\kappa_{11}$	$\kappa_{22}, \kappa_{33}$	$e_{111}$	$e_{122}, e_{133}$	$e_{212}, e_{313}$	
0.0151	0.0130	23.3	-6.5	17.0	

Table 1. Properties of the PZT-5H ceramics (polarized along  $x_1$  axis).

One of the most commonly used approaches to model the crack growth is an irreversible cohesive law with loading–unloading hysteresis. According to the cohesive zone model (CZM),

spontaneous polarization	$P^{sp}$	0.3	C/m <sup>2</sup>
coercive field strength	$E_c$	0.8	kV/mm
spontaneous strain	$\epsilon^{sp}$	0.3	%

Table 2. Nonlinear ferroelectric constants of the PZT-5H ceramics.

the material gradually loses its load-bearing capacity. Thus the whole damage process, starting from the crack formation until failure, can be modelled. Information about the developed electromechanical cyclic cohesive zone model (EMCCZM) can be found in [11] and is schematically presented in Fig. 4, right. Orange dots show different position on the traction-separation law (TSL)  $t(\delta)$  curve during material damage. TSL connects normalized effective traction  $t$  and separation  $\delta$ , introduced as following:

$$t = \sqrt{t_n^2 + t_r^2 + t_s^2}/t_0, \quad \delta = \sqrt{\langle \delta_n \rangle^2 + \delta_r^2 + \delta_s^2}/\delta_0. \quad (4)$$

Here  $\langle \delta_n \rangle = (\delta_n + |\delta_n|)/2$ ;  $t_0$  denotes maximum cohesive traction,  $\delta_0$  - critical separation at maximum cohesive traction; indices  $n, r$  and  $s$  stand for normal and two tangential quantities.

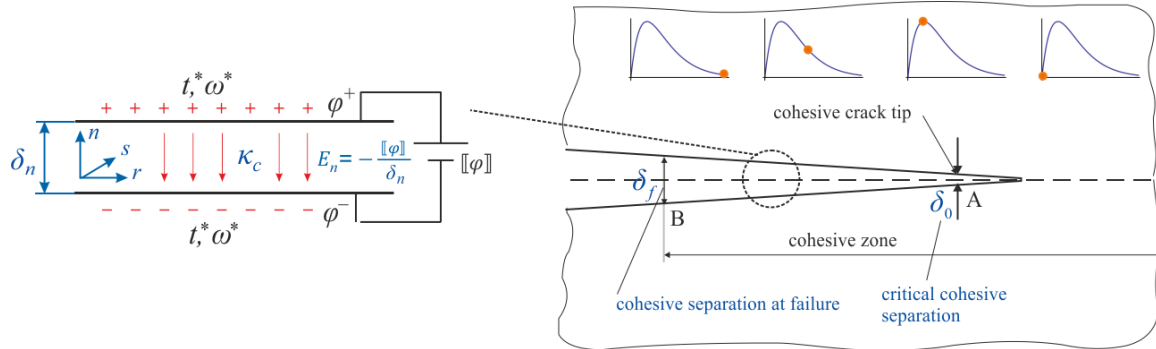


Figure 4. Parallel plate capacitor model (left) and cohesive zone approach (right).

Electrically, CZE has the behavior of a medium with limited dielectric permittivity  $\kappa$  [17]. With the accumulation of damage  $D$ , dielectric permittivity of the cohesive elements degrades

$$\kappa_c = (1 - D)\kappa_a + D\kappa_0 \quad (5)$$

and the dielectric displacement field  $D_n$  inside the CZE is defined as [11]:

$$D_n = -[(1 - D)\kappa_a + D\kappa_0] \frac{\phi^+ - \phi^-}{\Delta_0 + \delta_n}. \quad (6)$$

The CCZM captures damage accumulation during cycling with constant amplitude and distinguishes between active separation and endurance threshold using an evolution law of the following form [12]:

$$\dot{D} = (1 - D) \left( \frac{\delta}{1 - \log(1 - D)} \right)^r \langle \dot{\delta} \rangle \mathbf{H}(\delta - \delta_e), \quad (7)$$

where  $\mathbf{H}$  is the Heaviside step function. Thus formula (7) is appropriate for modeling piezo-electric ceramics degradation during exploitation loading.

An example of the CZE behavior during monotonic loading from an initially undamaged state and subsequent unloading-reloading cycles is presented in Fig. 5.

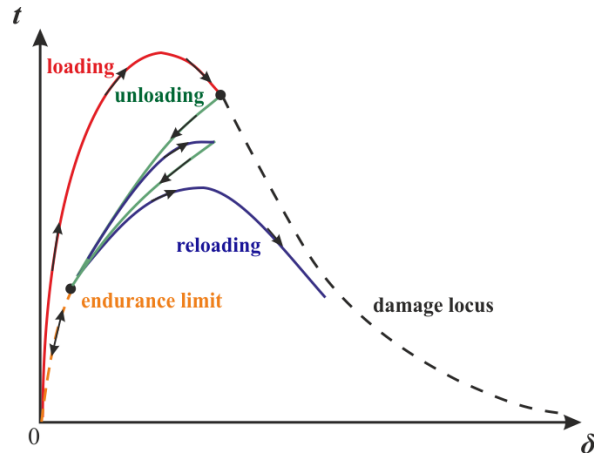


Figure 5. Response of CZE to initial monotonic loading followed by two unloading-reloading cycles according to the TSL.

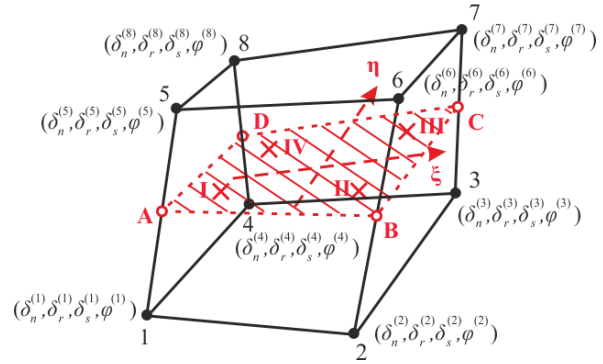


Figure 6. Illustration of EMCCZE; midplane values are marked in red.

The applied electromechanical cohesive elements consist of eight nodes and four integration points located in a midplane (see Fig. 6). Each IP has three mechanical and one electrical DOF. During electromechanical loading the upper and lower faces of CZE split in normal and/or tangential directions.

The properties of the EMCCZM are specified in Table 3.

fracture energy	$\Gamma_0$	2.34	N/m
maximum cohesive traction	$t_0$	100	MPa
critical separation	$\delta_0 = \Gamma_0 / (et_0)$	8.608	nm
thickness of a grain boundary	$\Delta_0$	5	nm
grain boundary permittivity @failure (air)	$\kappa_0$	$8.854 \cdot 10^{-6}$	$\mu\text{F/m}$
initial grain boundary permittivity	$\kappa_a = \kappa_0 \kappa_r$	0.006	$\mu\text{F/m}$

Table 3. Material constants of the cohesive zone.

### 3. Numerical simulation

The main aim of the present study is to investigate the damage initiation and accumulation in the MLA. The presence of an external frame results in the pre-stressed state in the MLA after the poling process.

In the numerical calculations, domain switching in the bulk material is accounted for by means of the non-linear ferroelectric model and damage is captured using the electromechanical cyclic CZE. Some simple examples as well as model validation can be found in [11] and [18]. The proposed approach adequately describes the processes occurring in the microstructure of smart ceramics.

The geometry of the MLA, the finite element mesh and the applied boundary conditions are presented in Fig. 7. In  $x_2$  direction plane strain conditions are applied; the cohesive elements have zero initial thickness. The external frame is modelled as a rod with a cross-section 2.5 times smaller than the cross-sectional area of the actuator. Assembling is being made aflush, afterwards pre-stress emerges during the poling process and remains subsequently due to the remanent strain.

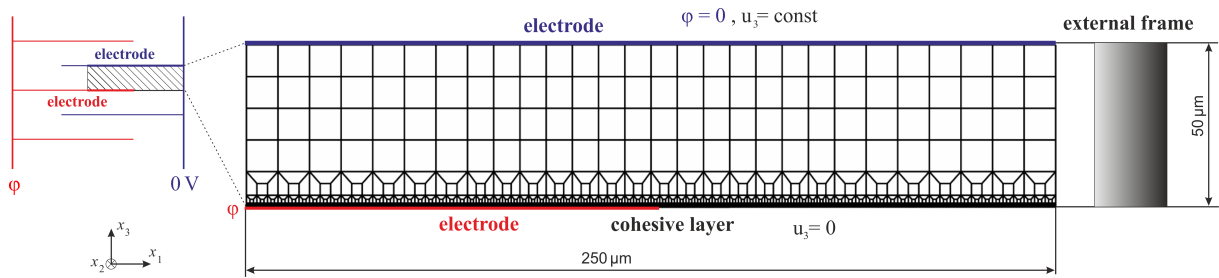


Figure 7. Finite element model of the actuator.

During poling, the electric potential  $\phi$  is increased from 0 to 100 V and then reduced to zero (see Fig. 8). This leads to an electric potential gradient growth up to 2 kV/mm ( $2.5E_c$ ) between the electrodes, which is enough to polarize the ceramics (Fig. 9).

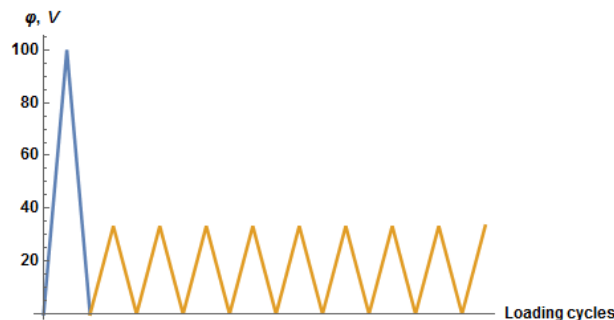


Figure 8. Diagram of the applied electric potential.

The polarization of the actuator at maximum electric voltage is illustrated in Fig. 9. The

PZT-5H ceramics is initially unpoled. Large number of vectors emerge along the electrode due to the high mesh density. Three different regions are easily observed:

- an active zone where after the poling process the ceramics is polarized along the  $x_3$  axis (left),
- an inactive zone which does not gain macroscopic piezoelectric properties and shows no electromechanical coupling (right),
- a transition zone in-between (center).

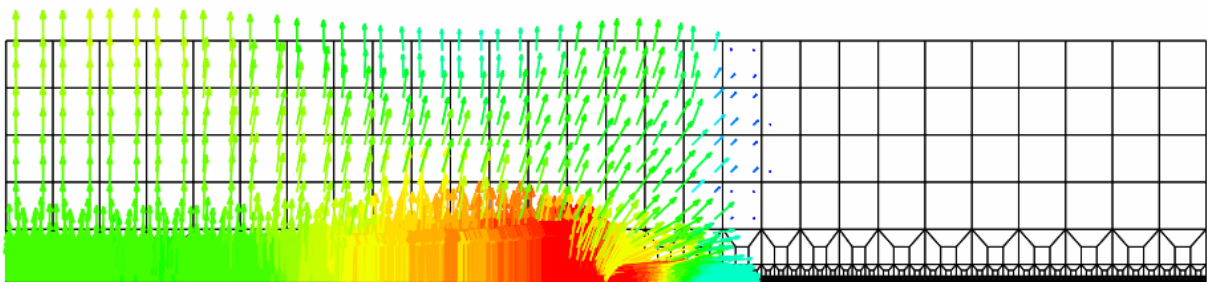


Figure 9. Vector plot showing polarization at maximum voltage during the poling process.

The electric potential along the electrode plane is plotted in Fig. 10 for the maximum voltage (red, dotted line) and after poling (red, solid line). The electrode ( $0 \dots 125 \mu\text{m}$ ), where the electric potential  $\phi = 100 \text{ V}$  is prescribed as the boundary condition, is followed by a gradual decay toward zero at the free edge of the actuator ( $125 \dots 250 \mu\text{m}$ ). After poling, the residual electric potential of about  $-5 \text{ V}$  is noticeable ahead of the electrode tip. Such electric behavior was first reported in [13]. Subsequent electric potential distribution during operational cyclic electric

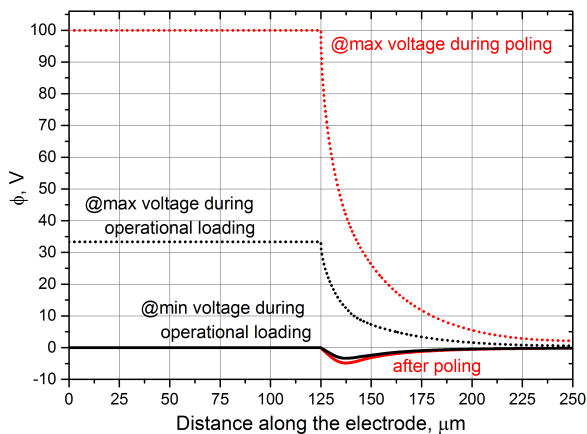


Figure 10. Electric potential along the electrode plane over the poling procedure and during exploitation.

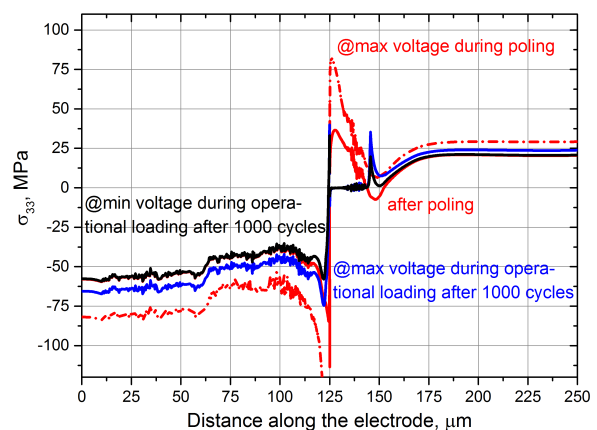


Figure 11. Change in stresses along the electrode plane during poling and exploitation.

loading (Fig. 8) is shown with the black dotted and solid lines for maximum and minimum applied voltage, respectively.

The red-coloured curves in Fig. 11 illustrate the normal stress distribution  $\sigma_{33}(x_1)$  in the cohesive layer during poling. The dash-dot red line shows stresses at maximum voltage, while the solid red line corresponds to the residual stresses after completion of the poling process. The analyses show distinguished regions of compression, tension and transition, which agree well with the previous simulations for the actuator without an external shell [13, 15]. The presence of the frame expectedly offsets the stresses in the MLA by a few tens of MPa downwards compared to the standard MLA, thus enhancing lifetime of the actuator and giving it the possibility to work in more severe operating conditions. The external frame experiences tensile loading at all times.

After completing the poling phase, cyclic electric voltage of the constant amplitude, which alternates from 0 to 33 V (see Fig. 8), is applied. Damage accumulates merely due to the electric cyclic loading. A contour plot for the damage, accumulated from 90 cycles, is shown in Fig. 12. For better visualisation, the deformation near the electrode tip is scaled 150 times. It is remarkable that the simulated cohesive elements' opening predicts the experimental observations [7], namely, the biggest separation and primarily damaged region lies ahead of the electrode edge (see Fig. 13, where the dark segment ahead of the electrode is an interlayer gap).

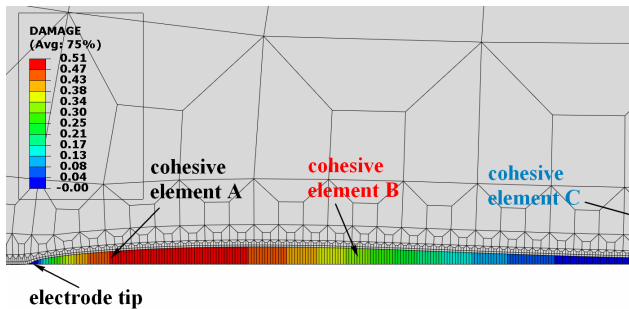


Figure 12. Damage accumulated after 90 electric cycles.

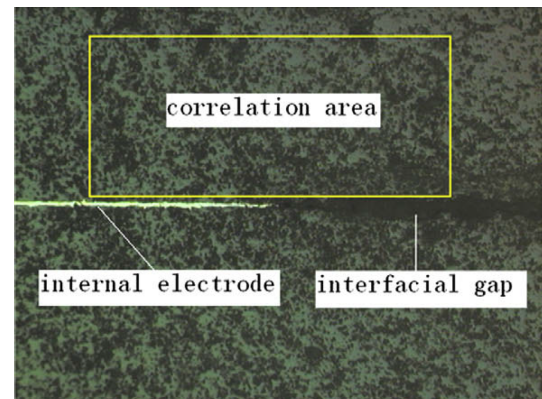


Figure 13. Speckle image of the crack due to electric loading (optical microscopy, taken from [7]).

Five characteristic points are selected for further illustration. Point A is located  $1 \mu\text{m}$  ahead of the electrode tip, points B and C - at  $4 \mu\text{m}$  and  $18 \mu\text{m}$ , respectively. Point D belongs to the right vertical face of the actuator, namely,  $x_{1D} = 250 \mu\text{m}$ .

Damage initiation and accumulation at the characteristic points A, B, C and D over 1000 cycles is shown in Fig. 14. According to the TSL, damage accumulates when cohesive traction is high enough to overcome endurance locus [12]. Below endurance limit, unloading/reloading curves coincide for an infinite number of cycles. Points A and B belong to the region where endurance locus is overcome during the poling process. During cyclic voltage this region continues to accumulate damage and extends with each cycle. At the point C damage initiates

after 500 cycles (Fig. 14, blue dotted line) which is seen as a propagation of the crack from the actuator tip. Further crack growth is restricted according to the stress distribution along the electrode, where a stress drop is observed (see Fig. 11, red curves). At the point D there is damage accumulation since the applied loading is insufficient to overcome the endurance limit in contrast to the MLA which is not pre-stressed [15].

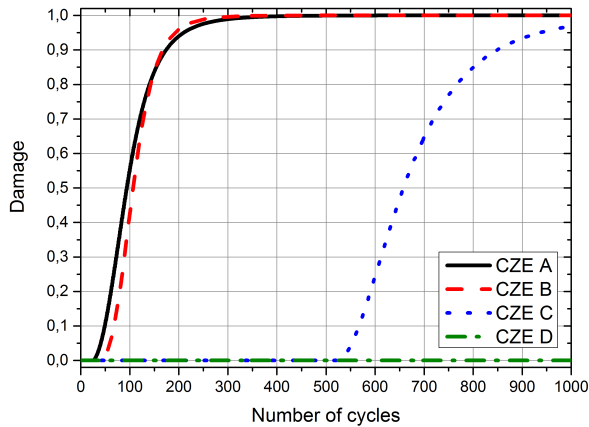


Figure 14. Damage accumulation shown at characteristic points along the electrode.

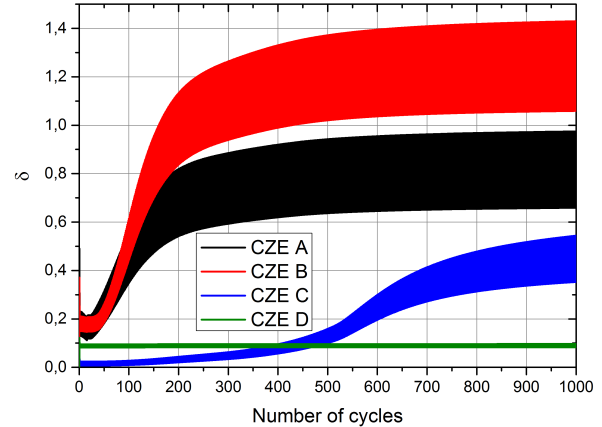


Figure 15. Change in normalized effective opening during cyclic electrical loading.

In Fig. 15 normalized effective opening variation is presented. At the points A and B opening is increasing as a consequence of diminishing resistance of the cohesive elements. Point B possesses bigger  $\delta$  magnitude after 100 cycles compared to the point A, since point A is closer to the compressed area at the left of the electrode tip (see Fig. 12). After 300 cycles effective opening growth in the cohesive elements slows down with complete damage at the points A and B. Opening at the point C is gradually increasing with damage accumulation as it is seen from Fig. 15. Since the rightmost region of the electrode is separated from the developing crack by a compressed area and no damage accumulation is observed, there is no change in normalized effective opening at the point D during electric cycling.

Figs. 16 and 17 illustrate oscillations of the normal tractions  $t_n$  as a result of electric cycling with constant amplitude. While Fig. 16 displays general view of the normal traction variation, Fig. 17 magnifies plots in selected cycling intervals since cycling loops at Fig. 16 are too condensed. Therefore two characteristic ranges are chosen and a break in the x-axis is introduced. One can readily see that during the poling process CZEs A and B experience an effective traction, which is lower than the maximum cohesive traction, but higher than the endurance limit. Cyclic electric loading as well leads to an effective traction in this cohesive elements which exceeds the endurance limit. From the beginning, peak value of the normal tractions and tractions' amplitude are observed at the point A. This leads to earlier damage initiation then at the point B (see Fig. 14). With continuing cycling, the damage zone is developing and peak stresses are shifting to the right, thus after 500 electric cycles the point C becomes the focus of the damage area. By this time the region containing points A and B is completely fractured (see Figs. 17, in-

terval (II) and 14). The peak tractions at the cohesive zone element C correspond to the damage origination at this point. It is also worth to observe the distribution of stresses along the electrode plane after 1000 cycles (Fig. 11): the peak of stresses is only slightly shifted to the right from the point C since the zone of compression is reached. No crack propagation is expected in the future, unless overloading happens, which may raise the stresses near the free edge of the actuator beyond the endurance limit. At the point D the mean value and the amplitude of the effective tractions remain constant, since stresses during poling and exploitation never exceed the endurance threshold and damage does not accumulate. It should be noticed, that for case of a fairly low endurance threshold, damage would accumulate at the point D as well.

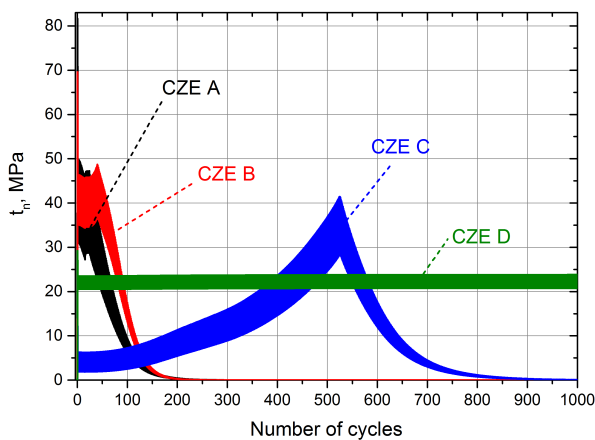


Figure 16. Effective traction variation during cyclic electric loading of constant amplitude: general view.

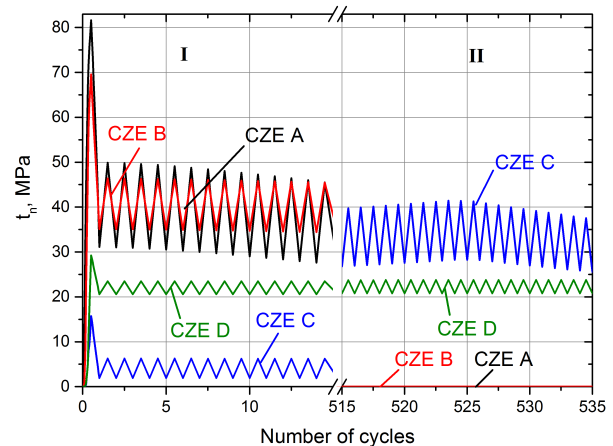


Figure 17. Effective traction variation during cyclic electric loading of constant amplitude: detailed view with a break in x-axis.

According to the traction-separation law, cyclic electric loading leads to unloading-reloading behavior in the cohesive elements (see Fig. 5). Fig. 19 presents actual traction-separation law at the characteristic points A, B, C and D over 1000 electric cycles. At the points A and B peak stresses during poling of the MLA are easily observed. On the contrary, poling process has no direct influence on the behavior of the point C, which is governed only by the initiation and expansion of the damaged region. At the point D movement according to the TSL is limited to the initial curve, since no damage is observed during cycling.

Fig. 18 illustrates cohesive zone opening, as well as specimen fracture, after 1000 electric cycles.

Fig. 20 represents the formation and expansion of the damaged zone during the operational cyclic electrical loading. After 50 cycles damage appears merely ahead of the electrode tip in the region, containing CZE A. With continuing cycling, damage magnitude is gradually increasing and after 400 cycles complete failure is reached at the points A and B. During this period damaged zone is progressing away from the electrode edge towards the right face of the actuator. This process continues up to the 700th cycle, when the compression region, generated

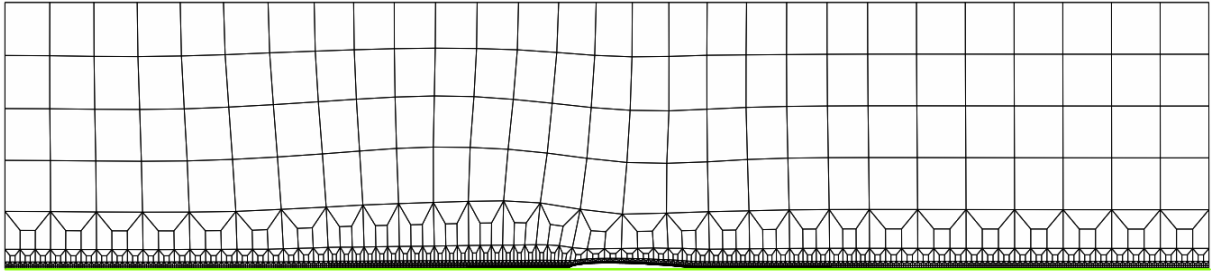


Figure 18. Damage of the actuator after 1000 electric cycles (magnified 200 times)

during the poling process, is reached (see Fig. 11). After that, damage accumulation is almost negligible and after 1000 cycle crack propagation is arrested.

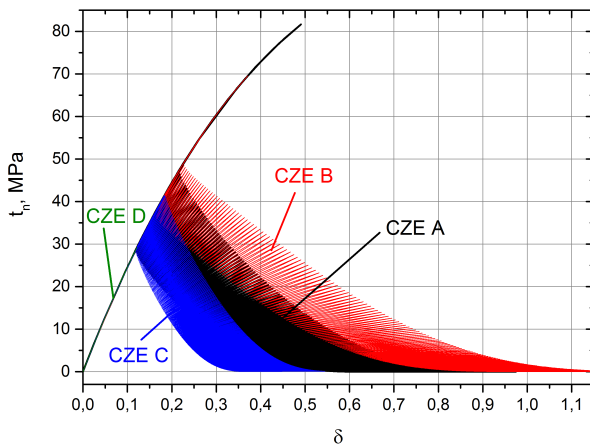


Figure 19. Traction-separation behavior in the cohesive layer as a result of electric loading.

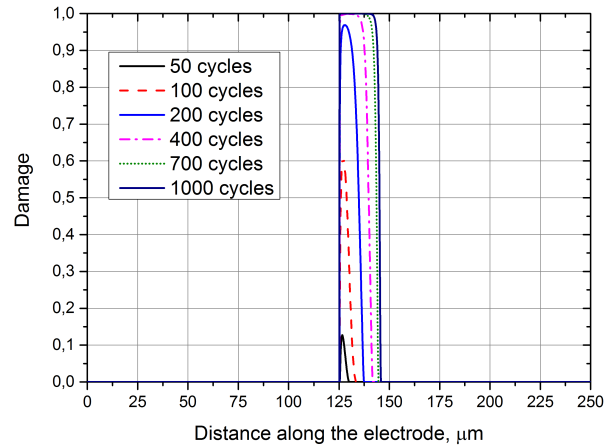


Figure 20. Damage initiation and accumulation along the electrode plane.

Thus, two different damage stages can be distinguished in the MLA.

The first one is associated with the poling process of the actuator. Domain reorientation due to the strong electric field between the electrodes leads to the formation of an active and inactive (in terms of piezoelectric response) zones (Fig. 9). These two regions and an external frame have to be balanced during deformation. This results in the occurrence of the compressed and stretched regions inside the MLA (Fig. 11) with the stretched outer frame. During the first step the endurance limit is surpassed in the region close to the actuator tip leading to the damage initiation.

At the second step, electric cycling is applied as under exploitation conditions. During this stage, damage accumulates in the region close to the electrode tip (Figs. 14 and 20) resulting in complete failure in the zone, depicted in Fig. 18.

#### 4. CONCLUSIONS

In the present paper, failure of the pre-stressed multi-layer actuator is studied by means of the finite element method. For the first time a coupled electromechanical simulation, combined with a cohesive zone model for the damage accumulation, is carried out. An advanced cyclic CZM is used together with a micromechanical domain switching approach. The cohesive zone technique allows to capture initiation and accumulation of damage, while domain switching modeling provides realistic simulation of the non-linear processes occurring in ferroelectric smart materials. In the electrical sense, the cohesive zone is being treated as a capacitor with finite electric permittivity, which degrades during damage accumulation. An important feature of the employed TSL is that electric cyclic loading of a constant amplitude leads to the damage increase, which can not be modeled with a monotonous TSL.

During the simulation, the poling process of the ceramics in the MLA is studied and electric potential distribution, polarization vectors, mechanical stresses are obtained and analysed. Piezoelectrically "active" and "inactive" zones are observed, with an external frame leading to the pre-stressed state of the actuator before exploitation. The formation and evolution of damage in the MLA is analyzed as a consequence of a purely cyclic electric loading. Results of our numerical simulations qualitatively coincide with the experimentally observed crack patterns.

It should be emphasized, that the mode of the crack initiation and growth is certainly dependent on the specific material, cohesive properties of the interface, stiffness of the external frame, type and magnitude of the electric in-service loading and poling technology.

Based on the current and forthcoming analyses, design suggestions can be proposed regarding the geometry of the actuators as well as their electromechanical properties, which will reduce the probability of MLA fracture.

#### 5. ACKNOWLEDGEMENTS

The research was partially funded by DFG under grant KU 929/20.

#### References

- [1] K. Uchino and S. Takahashi. Multilayer ceramic actuators. *Current Opinion in Solid State and Materials Science*, 1:698 – 705, 1996.
- [2] G.A. Schneider. Influence of electric field and mechanical stresses on the fracture of ferroelectrics. *Annual review of materials research*, 37:491 – 538, 2007.
- [3] M. Kuna. Fracture mechanics of piezoelectric materials - where are we right now? *Engineering Fracture Mechanics*, 77(2):309 – 326, 2010.
- [4] J.e. Huber, N.a. Fleck, C.M. Landis and R.M. McMeeking. A constitutive model for ferroelectric polycrystals. *Journal of the Mechanics and Physics of Solids*, 47(8):1663 – 1697, 1999.

- [5] A. Furuta and K. Uchino. Dynamic Observation of Crack Propagation in Piezoelectric Multilayer Actuators. *Journal of the American Ceramic Society*, 76(8):1615 — 1617, 1993.
- [6] S.L dos Santos e Lucato, D.C Lupascu, M Kamlah, J Rödel and C.S Lynch. Constraint-induced crack initiation at electrode edges in piezoelectric ceramics. *Acta Materialia*, 49(14):2751 – 2759, 2001.
- [7] X.J. Zhao, B. Liu and D.N. Fang. Study on electroelastic field concentration around the electrode tip in multilayer ferroelectric actuators of two designs and their optimizations. *International Journal of Plasticity*, 26(4):533 – 548, 2010.
- [8] I. Arias, S. Serebrinsky and M. Ortiz. A phenomenological cohesive model of ferroelectric fatigue. *Acta Materialia*, 54(4):975 – 984, 2006.
- [9] J. Utzinger, P. Steinmann and A. Menzel. On the simulation of cohesive fatigue effects in grain boundaries of a piezoelectric mesostructure. *International Journal of Solids and Structures*, 45(17):4687 – 4708, 2008.
- [10] C.V. Verhoosel and M.A. Gutiérrez. Modelling inter- and transgranular fracture in piezoelectric polycrystals. *Engineering Fracture Mechanics*, 76(6):742 – 760, 2009.
- [11] S. Kozinov, M. Kuna and S. Roth. A cohesive zone model for the electromechanical damage of piezoelectric/ferroelectric materials. *Smart Materials and Structures*, 23(5):055024, 2014.
- [12] S. Roth, G. Hütter and M. Kuna. Simulation of fatigue crack growth with a cyclic cohesive zone model. *International Journal of Fracture*, 188(1):23–45, 2014.
- [13] M. Kamlah and U. Boehle. Finite element analysis of piezoceramic components taking into account ferroelectric hysteresis behavior. *International Journal of Solids and Structures*, 38(4):605 – 633, 2001.
- [14] A. Abdollahi and I. Arias. Crack initiation patterns at electrode edges in multilayer ferroelectric actuators. *Smart Materials and Structures*, 21(9):094011, 2012.
- [15] S. Kozinov and M. Kuna. Simulation of damage in ferroelectric actuators by means of cohesive zone model. *[submitted for publication to Sensors and Actuators A: Physical]*, 2015.
- [16] S.C. Hwang and R.M. McMeeking. A finite element model of ferroelastic polycrystals. *International Journal of Solids and Structures*, 36(10):1541 – 1556, 1999.

- [17] H. Tian-Hu and S. Zi-Yuan. A new electric boundary condition of electric fracture mechanics and its applications. *Engineering Fracture Mechanics*, 47(6):793 – 802, 1994.
- [18] S. Kozinov, S. Roth and M. Kuna. Development of a cohesive model for damage simulation in ferroelectric materials subjected to electromechanical loading. *In: 11th World Congress on Computational Mechanics (WCCM XI)*. Ed. by Oñate E., Oliver J. and Huerta A., pages 4320–4331, 2014.